Journal of
Mechanical
Science and
Technology

Journal of Mechanical Science and Technology 21 (2007) 1819~1827

# Elongated bubble behavior during flow boiling in a microchannel

Cheol Huh*, Chi Woong Choi and Moo Hwan Kim

*Department of Mechanical Engineering, Pohang University of Science and Technology (POSTECH), San 31, Hyoja-dong, Nam-gu, Pohang, Kyoungbuk 790-784, Korea*

(Manuscript Received May 7, 2007; Revised July 11, 2007; Accepted July 11, 2007)

**Abstract**

Elongated bubble flow is a unique flow pattern that occurs during flow boiling in a microchannel. The incepted bubbles quickly grow to the channel size and form long elongated bubbles due to the confinement of the microchannel. The flow regimes and heat transfer coefficients in the microchannel are closely related to the elongated bubble behavior. Numerical and experimental investigations were performed to study the behavior of elongated bubbles and their effect on flow boiling. Elongated bubble growth in a 100-μm-diameter microchannel was calculated by using a two-zone model, while flow visualization of elongated bubble behavior was obtained with a high-speed CCD camera. Comparisons between the calculated results and experimental observations showed that the growth of the elongated bubble was governed by the evaporation of the thin liquid film that formed between the vapor core and the heated channel wall.

*Keywords*: Elongated bubble; Two-zone model; Flow boiling heat transfer; Microchannel; Two-phase flow; Flow visualization

## 1. Introduction

Flow boiling in microchannels is one of the most promising research areas today due to advances in microchannel heat exchangers and micro-devices such as MEMS-based micro pumps. In particular, the formation and behavior of micro vapor bubbles during microscale phase-change heat transfer has been extensively studied. The incepted bubbles quickly grow to the channel size and form very long elongated bubbles due to the confinement effect in a microchannel. The formation and growth behavior of these bubbles affect not only the heat transfer but also the flow patterns, contributing to the overall pressure drop and boiling heat transfer of the entire microscale flow boiling phenomena. However, we lack an understanding of the elongated bubble behavior, and further research is required to clarify its role in the heat transfer mechanism.

Cornwell and Kew [1] proposed three microchannel flow regimes: (i) isolated bubble flow which is similar to bubbly flow in a large channel, (ii) confined bubble flow which has elongated bubbles, and (iii) annular-slug flow. They visualized boiling R-113 flow in multiple minichannels with cross-sectional area of 1.2x0.9 $mm^2$. As the confined bubbles expand, liquid in the slugs between them is deposited on the channel walls and the flow becomes annular with random, irregular slugs of liquid interspersed with the vapor.

Many studies have numerically investigated the behavior of bubbles in a microchannel. Different models can be classified by the types of equations, which is the starting point of interesting topics. Numerical simulation of bubble growth and behavior in a microchannel using the level set method was carried out by Mukherjee and Kandlikar [2]. They showed that the flow reversal described by Kandlikar et al. [3] can be suppressed by using restrictors at the

*Corresponding author. Tel.: +82 54 279 5911, Fax.: +82 54 279 3199
E-mail address: dratom@postech.ac.kr

inlet. Bubble behavior during evaporation and condensation in upward slug flow was simulated by using the volume of fluid (VOF) method by Kumagai et al. [4], while Yang et al. [5] simulated bubble behavior under adiabatic conditions using the lattice Boltzmann method (LBM). Since these models are based on partial differential equations (PDEs), they can be evaluated by using a computational fluid dynamics (CFD) solver. Models based on ordinary differential equations (ODEs) are derived from the liquid film thickness. The researches of Qu et al. [6] and Park et al. [7, 8] were focused on the heat transfer in the thin liquid film, known as microlayer, which originates from the single bubble growth in pool boiling. Their models used the augmented Young-Laplace equation, proposed by Potash and Wayner [9]. To develop a heat transfer model based on the flow pattern, a thin liquid film evaporation model of elongated bubble in microchannel was proposed by Jacobi and Thome [10]. They assumed that the incepted bubbles quickly grew to the channel size such that successive elongated bubbles were formed. The elongated bubbles were confined by the channel, forming a thin film of liquid between the bubble and the channel wall. A detailed explanation of their two-zone model is given in the numerical analysis section of this paper.

In this study, we examined the effect of elongated bubble behavior in microchannel flow boiling. The elongated bubble growth in a 100-μm-diameter microchannel was calculated by using a two-zone model. Flow visualization of elongated bubble behavior was performed with a high-speed CCD camera, and the results were compared with numerically calculated data.

## 2. Experiments

### *2.1 Experimental apparatus*

We used a microscale heater array to supply thermal energy to the working fluid and to measure the local heated wall temperature. A series of platinum 20-μm-wide microheaters were deposited inside the microchannel in the flow direction. We used a horizontal rectangular microchannel having about 100-μm-hydraulic diameter in this study. We fabricated a parylene-coated polydimethylsiloxane (PDMS) microchannel with a 100-μm-wide and 100-μm-high channel cross section (i.e., aspect ratio is one) by using the replica molding technique. The dimensional uncertainty of the microchannel was $\pm 2$ μm due to the coating of parylene on PDMS. Because pure PDMS has unfavorable characteristics such as high permeability to some gases and elastic behavior, conformal coating of parylene C dimer (di-chloro-di-para-xylylene) on the internal surface of the microchannel was performed. The parylene polymers were deposited from the vapor phase by a process which in some respects resembles vacuum metalizing.

Parylene film has a low permeability to moisture and gases such as nitrogen, oxygen and carbon dioxide. The barrier properties of the parylene on moisture vapor transmission and gas permeability are superior to almost all polymeric materials such as epoxides [11]. In addition, it has been found that Young's modulus, tensile strength and Rockwell hardness of parylene are considerably greater than those of epoxides, silicones and urethanes [11]. Therefore, a parylene-coated PDMS microchannel is sufficient to provide consistent resistance to deforming.

The working fluid flow rate and heat flux were too small to measure by conventional test methods. Instead, new measurement techniques were developed for flow boiling heat transfer inside a single microchannel. Each microheater was heated by using the Joule effect with a DC current. To evaluate the heat input from the microheaters, the voltage and current in each microheater were measured. And each microheater had a central serpentine pattern 20 μm wide and four lead line patterns 2.54 mm wide. It is believed that most of the heat generated by the platinum is concentrated in the area of the central serpentine pattern corresponding to the microheater due to the very large line width ratio of the lead line

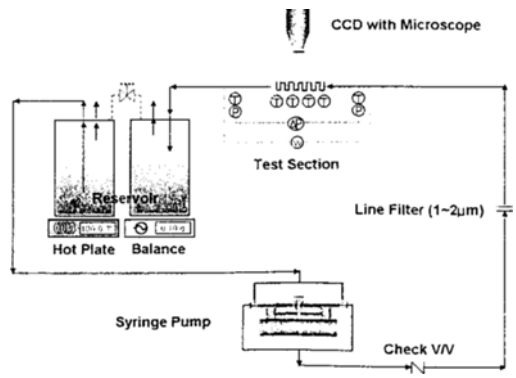


Fig. 1. Schematic diagram of the experimental apparatus [3].

pattern to the serpentine pattern. In addition, each microheater has four lead lines (two for measurement of electric voltage and two for electric power supply and current measurement); it is possible to apply the Kelvin four-wire resistance measurement principle. Therefore, we can avoid the measurement uncertainties caused by wire resistance.

Since a linear relationship exists between resistance and temperature in platinum, platinum microheaters perform as both heaters and temperature sensors. To quantify the relationship between temperature and the resistance of each microheater, each microheater was calibrated in a constant-temperature convection oven after sufficient time was allowed to achieve thermodynamic equilibrium. Each microheater showed a fairly good linear relationship between temperature and resistance.

The flow rate of the working fluid, as low as a few drops of water per minute, was measured by reading the mass gradient with time from the electronic balance on which the outlet reservoir was installed. The returning liquid and vapor mixture accumulated in the outlet reservoir and water vapor condensed.

A conceptual schematic diagram of the measurement techniques is depicted in Fig. 1. A detailed description of the experimental apparatus, including the test section, can be found in Huh et al. [12]. Deionized and degassed water was used as the working fluid.

### *2.2 Flow visualization*

A high-speed CCD camera with a microscope was installed above the test section to obtain a real-time flow visualization of the elongated bubble growth and elongated bubble flow for flow boiling in a microchannel. During the experiments, flow pattern images were captured at a rate of 30,000 frames per second.

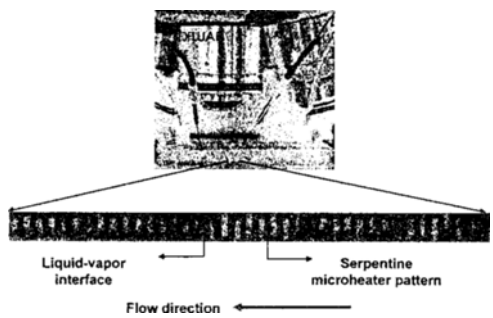


Fig. 2. Flow visualization apparatus.

The Illumination light for the high-speed images was passed from the bottom of the test section to the objective lens of the microscope through the test section. A transparent PDMS microchannel was used to provide simultaneous visualizations during the experiments. The test section and flow visualization devices are shown in Fig. 2. The dark serpentine pattern shown underneath the liquid and vapor phases represents the 20-μm-line-width platinum microheaters.

### *2.3 Data reduction*

The heat generated in each microheater was estimated from Eq. (1).

$$q = VI \tag{1}$$

where, V and I are the measured electric voltage and electric current, respectively. The effective heat fluxes in the microheaters were calculated from net heat input by subtracting the heat loss based on the effective heating area.

$$q_{eff} = q - q_{loss} \tag{2}$$

$$q'' = \frac{q_{eff}}{W_{ch} L_{ch}} \tag{3}$$

where, $W_{ch}$ and $L_{ch}$ are the width and the length of the microchannel so that the denominator of Eq. (3) represents the planform area of the microchannel. The heat losses were evaluated from the relationship between the temperature of heated surface $T_h$, the temperature of outer wall $T_{ow}$, and the heat input $q$.

The uncertainties for the experimental variables were evaluated by using Holman's method [13]. The uncertainties of the measured temperature and pressure at the inlet or outlet of the test section were ± 0.1°C and ± 0.76kPa. The uncertainties of the mass flux and heat flux were ± 1.09% and ± 2.74%, respectively.

## 3. Numerical analysis

### *3.1 Thin film evaporation model for elongated bubbles*

We used Jacobi and Thome's [10] two-zone model to simulate elongated bubble behavior in the microchannel. Assume a pair of elongated bubble and liquid slug flow in the microchannel with a hydraulic

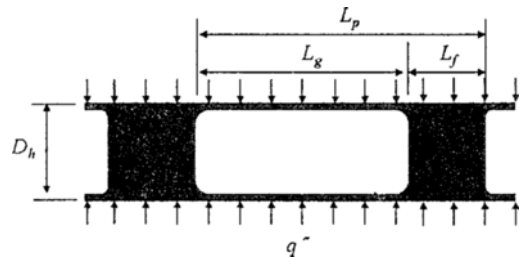


Fig. 3. The elongated bubble/liquid slug flow described by the Jacobi and Thome model [10].

diameter of $D_h$. Under a constant heat flux, the length of the elongated bubble $L_g$ increases and the length of the liquid slug $L_f$ decreases. After inception of the bubbles at the nucleation site, they quickly fill the entire microchannel and grow in the flow direction due to the confinement effect of the microchannel. Jacobi and Thome assumed that up to the instant of bubble detachment, the elongated bubble and liquid slug flow passed the microchannel at the liquid velocity, over each period of bubble generation a pair.

$$L_p(t=0) = L_{po} = \frac{\tau m}{\rho_f} \tag{4}$$

$$L_g(t=0) = L_{go} = D_h \tag{5}$$

$$L_p(t) = L_g(t) + L_f(t) \tag{6}$$

Using an energy balance and mass conservation, the coupled differential equations for the vapor and liquid length can be derived:

$$\frac{dL_g}{dt} = \frac{q''D_h\left(L_g(t)+L_f(t)\right)}{\rho_g\left(R-\delta_o\right)^2 i_{fg}} \tag{7}$$

$$\frac{dL_f}{dt} = -\frac{q''D_h\left(L_g(t)+L_f(t)\right)}{\rho_f\left(R-\delta_o\right)^2 i_{fg}} \tag{8}$$

where $\delta_0$ is the initial liquid film thickness.

### *3.2 Period of elongated bubble and liquid slug pair generation*

The two-zone model applies a conduction-limited timescale to estimate the period of time between the generations of successive elongated bubble/liquid slug pairs. These timescales were derived from the bubble growth behavior governed by the conduction-limited model [14] in a uni-formly superheated liquid,

$$r(t) = Ja\left(\frac{12\alpha_f \tau}{\pi}\right) \tag{9}$$

$$\tau = \left(\frac{R\rho_g i_{fg}}{\rho_f c_{P,f}\Delta T_{sat}}\right)^2 \frac{\pi}{12\alpha_f} \tag{10}$$

$$Ja = \frac{\rho_f c_{P,f}\Delta T_{sat}}{\rho_g i_{fg}} \tag{11}$$

where Ja is the Jakob number, $\alpha_f$ is the thermal diffusivity of the liquid, r is the bubble radius, and $T_{sat}$ is the superheat of the heated channel. Their timescale was the period required for the bubble to grow to the channel radius. Therefore, the time period $\tau$ for successive bubble formations, or the sweeping frequency of the elongated bubble/liquid slug pair, was a function of the bubble radius and the wall superheat. In elongated bubble flow, the bubble radius given by Eq. (9) is the channel radius. With these relations, the timescale $\tau$ for the experimental conditions (order of $10^{-7}$~$10^{-6}$) was too small to proceed with the bubble growth calculations due to the very small hydraulic diameter ($D_h$=100 μm). Therefore, the bubble departure frequency observed during the experiment was used for the numerical calculations in this study. A detailed method for determining the bubble departure frequency will be discussed in the following section.

Since the bubble frequency reported by the conduction-limited model [14] was very small, the initial length of the elongated bubble/liquid slug pair was also small. These small frequencies and initial lengths also made it difficult to perform the numerical calculations. To reconcile these numerical difficulties, we used the observed initial bubble and liquid slug lengths from the experiments.

## 4. Results

### *4.1 Bubble frequency*

To obtain the bubble departure frequency in the microchannel, visualizations of the bubble inception, growth, and departure were carried out during the experiments.

Fig. 4 shows the sequential images of the bubble behavior for a mass flux G=130 kg/m$^2$s and a heat flux q"=195 kW/m$^2$. The images were captured at a

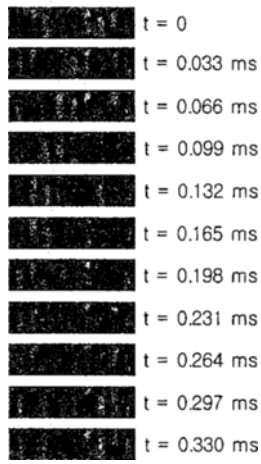


Fig. 4. Inception, growth and departure of single bubble at G=130 kg/m$^2$s and q"=195 kW/m$^2$.

rate of 30,000 frames per second. The time span between successive bubble inceptions was $3.3 \cdot 10^{-4}$ s, which is longer than the value estimated by using the conduction-limited model [14], Eq. (6), for a given hydraulic diameter.

Zuber [15] suggested the following relationship for the mean bubble departure diameter $D_d$ and bubble departure frequency f:

$$fD_d = 0.59\left[\frac{\sigma g(\rho_f - \rho_g)}{\rho_f^2}\right]^{1/4} \quad (12)$$

The bubble departure frequency obtained by using Zuber's [15] model and the experimentally measured values gives the same order of magnitude of $10^{-4}$. The departure diameter of the bubble in the microchannel was approximately half the hydraulic diameter, as shown in Fig. 4. Since Zuber's model gives a similar bubble departure diameter by using the actual measured bubble frequency, we used it to calculate the bubble growth behavior (Eqs. (5) and (6)).

### *4.2 Initial length of an elongated bubble*

The length of the elongated bubble can be calculated by using the differential equations given by Eqs. (7) and (8), and the initial conditions given by Eqs. (4)~(6). However, a shorter period, that is, a higher frequency, of the elongated bubble and liquid slug generation given by the conduction-limited model yields different elongated bubble growth rates

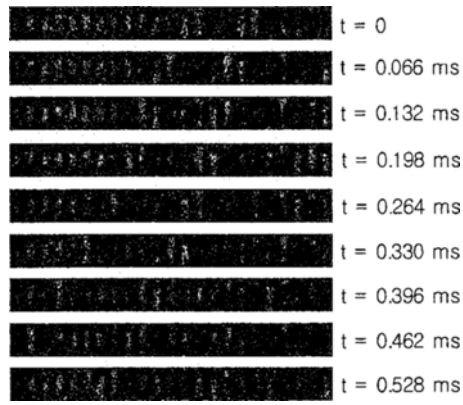


Fig. 5. Formation of an elongated bubble at G=130 kg/m$^2$s and q"=195 kW/m$^2$.

compared to experimental results. This discrepancy arises because the conduction-limited model was derived for superheated pool boiling conditions, whereas the thermodynamic state of the bulk fluid flow is not superheated in the present microchannel. Therefore, we used the measured initial length of the elongated bubble in this study. The initial length of the elongated bubble/liquid slug pair was evaluated from the flow visualization results.

### *4.3 Formation of an elongated bubble*

Elongated bubble flow is a unique flow pattern encountered in microscale flow boiling. A single bubble incepted in the microchannel grows, departs, quickly fills the entire cross section of the channel, and finally forms an elongated bubble. The flow regimes and heat transfer coefficient are closely correlated with the elongated bubble behavior. Fig. 5 shows the formation of elongated bubble in the microchannel. The confinement of the microchannel wall produced long elongated bubbles.

### *4.4 Growth of an elongated bubble*

As shown in Figs. 5 and 6, an elongated bubble is important both from scientific and practical points of view in relation to microscale fluid flow and heat transfer problems. After the departure of the bubble from the incepted cavities, the elongated bubble behavior corresponds to heat transfer mechanism. In particular, the growth of the elongated bubble in the flow direction, both upstream and downstream, is governed by the major heat transfer mechanism in microchannel flow boiling.

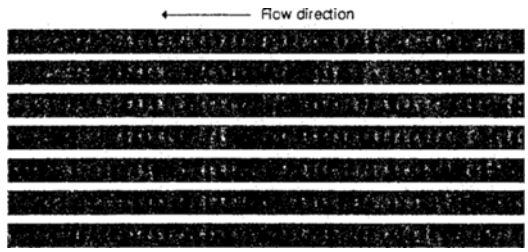


Fig. 6. Growth of an elongated bubble at G=130 kg/m$^2$s and q"=195 kW/m$^2$ (time span between successive images =1.0·10$^{-4}$ s)

Fig. 6 shows sequential images of elongated bubble growth at a mass flux G=130 kg/m$^2$s and a heat flux q"=195 kW/m$^2$. The images were captured at 30,000 frames per second and the time span between successive images was 1.0·10$^{-4}$ s. Different movements of the leading and trailing liquid-vapor interfaces were observed, indicating the elongated bubble grew not only in the flow direction but also counter to the bulk fluid flow direction.

A numerical calculation of the elongated bubble growth was performed by using Eqs. (7) and (8). The initial conditions, which are the length of the elongated bubble/liquid slug pair, were obtained from the visualization results shown in Fig. 6. One of the adjustable parameters, the nucleation superheat, was obtained from the measured heated wall temperature. This was possible because the platinum microheaters had a linear relationship between temperature and electrical resistance. Therefore, it is possible to get local superheat condition.

The two-zone model [10] was originally developed for a circular microchannel under axially uniform heating conditions. However, the present rectangular microchannel was under non-uniform circumferential heating conditions. Since the PDMS has a thermal conductivity as low as 0.15 W/mK, the side and top wall of the microchannel could be considered insulated. This modification to the heated area was considered in the numerical calculations.

In a circular uniformly heated microchannel, the heat transfer area is described as the internal surface area (i.e., product of circumference and length). On the other hand, the heat transfer area in single-side heated rectangular microchannel can be expressed as a product of the width and length of the heated channel wall only when the non-heated wall can be treated as insulated state. Therefore, the coupled differential equations for the vapor and liquid can be modified:

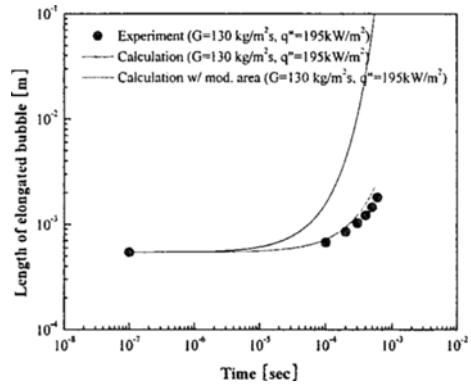


Fig. 7. Length of an elongated bubble at G=130 kg/m$^2$s and q"=195 kW/m$^2$.

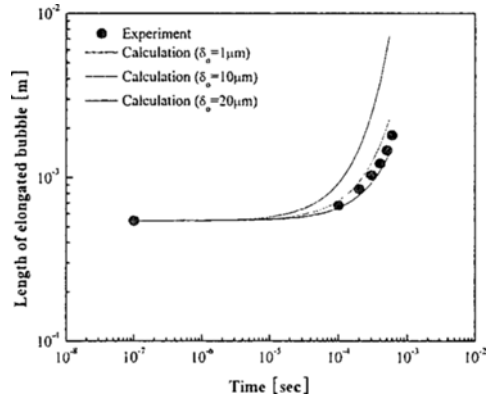


Fig. 8. Effect of the initial film thickness on the elongated bubble growth at G=130 kg/m$^2$s and q"=195 kW/m$^2$.

$$\frac{dL_g}{dt} = \frac{q'' W_{ch}\left(L_g(t) + L_f(t)\right)}{\rho_g \pi \left(R - \delta_o\right)^2 i_{fg}} \tag{13}$$

$$\frac{dL_f}{dt} = -\frac{q'' W_{ch}\left(L_g(t) + L_f(t)\right)}{\rho_f \pi \left(R - \delta_o\right)^2 i_{fg}} \tag{14}$$

The elongated bubble lengths are compared to the experimental data in Fig. 7. The modified heating area calculations represented the experimental behavior well. Therefore, this modification was applied to the following calculations. The other variable parameter, the initial film thickness, was assumed to be one-tenth of the hydraulic diameter.

At present, the initial film thickness is difficult to measure directly. Fig. 8 shows the effect of the initial liquid film thickness on the elongated bubble

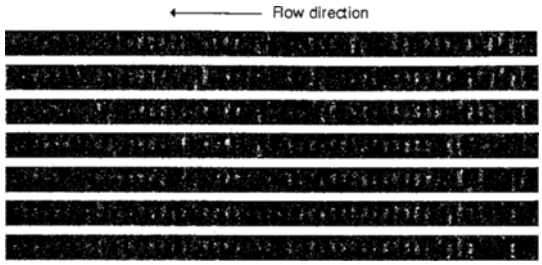


Fig. 9. Growth of an elongated bubble at G=136 kg/m$^2$s and q"=190 kW/m$^2$ (time span between successive images = $2.0 \cdot 10^{-4}$ s).

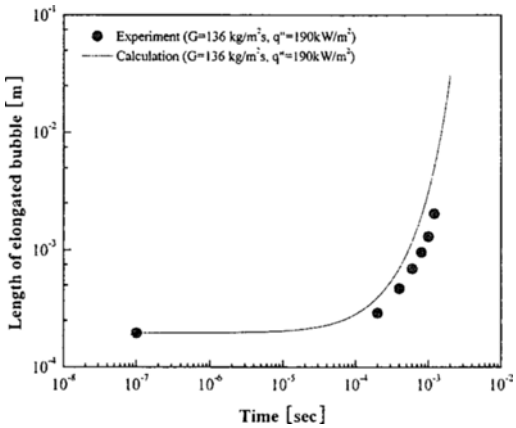


Fig. 10. Length of an elongated bubble at G=136 kg/m$^2$s and q"=190 kW/m$^2$.

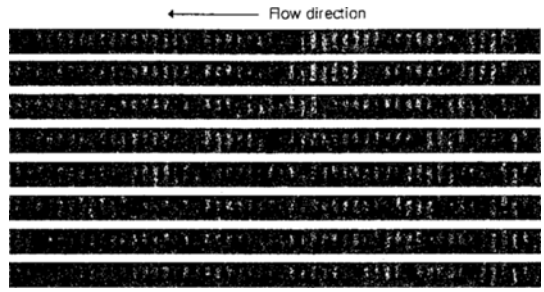


Fig. 11. Growth of an elongated bubble at G=150 kg/m$^2$s and q"=176 kW/m$^2$ (time span between successive images = $2.0 \cdot 10^{-4}$ s).

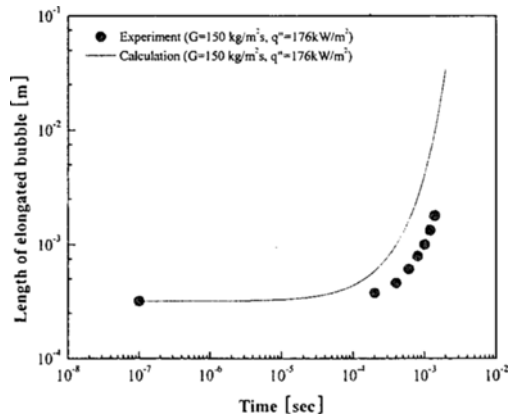


Fig. 12. Length of an elongated bubble at G=150 kg/m$^2$s and q"=176 kW/m$^2$.

growth behavior. The initial film thicknesses between 1 and 10 μm showed similar behaviors; however, thicker initial film thicknesses produced unreasonable bubble growth estimations.

Fig. 9 shows the elongated bubble growth at a mass flux G=136 kg/m$^2$s and a heat flux q"=190 kW/m$^2$. The images were captured at 30,000 frames per second and the time span between successive images was $2.0 \cdot 10^{-4}$ s. Fig. 10 shows that the behavior of the elongated bubble length obtained from the experiments was similar to that from the numerical calculations. However, larger mass flux and smaller heat flux conditions yielded a higher growth rate in the calculations compared to that given in Fig. 7.

Fig. 11 shows the elongated bubble growth at a mass flux G=150 kg/m$^2$s and a heat flux q"=176 kW/m$^2$. The images were captured at 30,000 frames per second and the time span between successive images was $2.0 \cdot 10^{-4}$ s. Fig. 12 compares the elongated bubble length obtained from experiments with that obtained from the numerical calculations. The numerical calculations predicted a higher growth rate than observed in the experiments.

As the mass flux increased and the heat flux decreased, the calculated results gave a higher growth rate for the elongated bubble. This difference implies that the numerical two-zone model predicted fast elongated bubble growth behavior compared to experiment. In other words, the two-zone model did not provide a reliable prediction capability as the vapor fraction decreased. On the other hand, the higher vapor fractions produced a thin liquid film flow along the heated wall and vapor flow in the core of microchannel, so that the thin liquid film evaporation in the two-zone model could predict the elongated bubble behavior.

## 5. Conclusions

Flow regimes and heat transfer mechanisms in a microchannel are closely correlated with the elon-

gated bubble behavior. Numerical and experimental investigations of flow boiling of water in a horizontal single microchannel ($D_h$=100 μm) were presented in this study. The elongated bubble growth behavior in a microchannel was analyzed by comparing experimental observations and numerical calculations under experimental initial conditions.

Our results are summarized as follows.

1. The bubble departure frequency could be predicted with Zuber's model.

2. The elongated bubbles grown from single bubbles dominated the major flow regimes and heat transfer mechanism.

3. The growth behavior of the long elongated bubbles was governed by thin film evaporation.

4. In elongated bubble flow regime, the two-zone model represented the bubble behavior well as the vapor fraction increased. However, the two-zone model did not provide a reliable prediction capability as the vapor fraction decreased.

5. Most actual microchannel devices have square or trapezoidal cross sections. Therefore, to make more useful and accurate predictions, the following modifications to the model are advised:

- use different film profiles inside the microchannel, especially at corners of the channel wall, and
- use a circumferentially nonuniform thermal boundary condition due to the single or triple wall heating conditions.

## Acknowledgements

This study was supported by the Program for Training Graduate Students in the Regional Innovation and Global Partnership Program of the Korean government.

## Nomenclature

$c_p$ : Specific heat, J/kgK
D : Diameter, m
f : Frequency, 1/s
g : Gravitational acceleration, m/s$^2$
$i_{fg}$ : Latent heat, J/kg
Ja : Jacob number, -
L : Length, m
m : Mass flux, kg/m$^2$s
$q''$ : Heat flux, W/m$^2$
R : Channel radius, m
t : Time, s
W : Width, m
α : Thermal diffusivity, W/mK
$\Delta T_{sat}$ : Wall superheat, K
ρ : Density, kg/m$^3$
σ : Surface tension, Nm
τ : Time period, s

### *Subscripts*

ch : Channel
d : Departure
eff : Effective
f : Liquid phase
g : Gas phase
h : Hydraulic

### *loss heat loss*

o : Initial state
p : Pair

## References

[1] K. Cornwell and P. A. Kew, Boiling in small parallel channels, *Proc. of CEC Conference on Energy Efficiency in Process Technology.* 22 (1992) 624-638.

[2] Mukherjee and S. G. Kandlikar, Numerical study of the effect of inlet constriction on bubble growth during flow boiling in microchannels, 3rd International Conference on Microchannels and Minichannels, ICMM2005, (2005) 75-143.

[3] S. G. Kandlika, M. E. Steinke, S. Tian and L. A. Campbell, High-speed photographic observation of flow boiling of water in parallel minichannels, National Heat Transfer Conference, ASME (2001).

[4] K. Kumagai, H. Iwai, H. Yoshida and M. Kuno, Study of slug inside vertical capillaries with phase change, 4th International Conference on Nanochannels, Microchannels and Minichannels (2006) 96-152.

[5] Z. L. Yang, B. Palm and B. R. Sehgal, Numerical simulation of bubbly two-phase flow in narrow channel, *Int. J. Heat Mass Transfer.* 45 (2002) 631-639.

[6] W. Qu and T. Ma, Effect of radius and heat transfer on the profile of evaporating thin liquid film and meniscus in capillary tubes, *Int. J. Heat Mass Transfer.* 45 (2002) 1879-1887.

[7] K. W. Park and K. S. Lee, Flow and heat transfer characteristics of the evaporating extended meniscus in a micro-capillary channel, *Int. J. Heat*

*Mass Transfer*. 46 (2003) 4587-4594.

[8] K. W. Park, Noh, K. J. and K. S. Lee, Transport phenomena in the thin film region of a microchannel, *Int. J. Heat Mass Transfer*. 46 (2003) 2381-2388.

[9] M. Potash JR. and P. C. Wayner JR., Evaporation from a two-dimensional extended Meniscus, *Int. J. Heat Mass Transfer*. 15 (1972) 1851-1863.

[10] M. Jacobi and J. R. Thome, Heat transfer model for evaporation of elongated Bubble Flows in Microchannels, *J. Heat Transfer.* 124 (2002) 1131-1136.

[11] Special coating systems, Parylene knowledge; specifications and properties, http:// www. scscoatings.com/parylene_knowledge/specifications.cfm (2007)

[12] C. Huh, J. B. Kim and M. H. Kim, Flow pattern transition instability during flow boiling in a single microchannel, *Int. J. Heat Mass Transfer*. 50 (2007) 1049-1060.

[13] J. P. Holman, *Experimental Methods for Engineers*, McGraw-Hill, New York, (2001).

[14] M. Plesset and S. A. Zwick, The growth of vapor bubbles in superheated liquids, *J. Appl. Phys*. 25 (1954) 493-500.

[15] N. Zuber, Nucleate boiling the region of isolated bubble-similarity with natural convection, *Int. J. Heat Mass Transfer*. 6 (1963) 53-65.